VOLUME 35 | SUPPLEMENT 2 | MARCH 2022

MODERN PATHOLOGY

ABSTRACTS (1089–1110)

NEUROPATHOLOGY AND OPHTHALMIC PATHOLOGY

2022

USCAP 111TH ANNUAL MEETING

REAL INTELLIGENCE

MARCH 19–24, 2022 LOS ANGELES, CALIFORNIA

Published by
SPRINGER NATURE
www.ModernPathology.org

USCAP Creating a Better Pathologist
AN OFFICIAL JOURNAL OF THE UNITED STATES AND CANADIAN ACADEMY OF PATHOLOGY

EDUCATION COMMITTEE

Rhonda K. Yantiss
Chair

Kristin C. Jensen
Chair, CME Subcommittee

Laura C. Collins
Chair, Interactive Microscopy Subcommittee

Yuri Fedoriw
Short Course Coordinator

Ilan Weinreb
Chair, Subcommittee for Unique Live Course Offerings

Carla L. Ellis
Chair, DEI Subcommittee

Adebowale J. Adeniran
Kimberly H. Allison
Sarah M. Dry
William C. Faquin
Karen J. Fritchie
Jennifer B. Gordetsky
Levon Katsakhyan, Pathologist-in-Training
Melinda J. Lerwill
M. Beatriz S. Lopes
Julia R. Naso, Pathologist-in-Training
Liron Pantanowitz
Carlos Parra-Herran
Rajiv M. Patel
Charles "Matt" Quick
David F. Schaeffer
Lynette M. Sholl
Olga K. Weinberg
Maria Westerhoff

ABSTRACT REVIEW BOARD

Benjamin Adam
Oyedele Adeyi
Mariam Priya Alexander
Daniela Allende
Catalina Amador
Vijayalakshmi Ananthanarayanan
Tatjana Antic
Manju Aron
Roberto Barrios
Gregory R. Bean
Govind Bhagat
Luis Zabala Blanco
Michael Bonert
Alain C. Borczuk
Tamar C. Brandler
Eric Jason Burks
Kelly J. Butnor
Sarah M. Calkins
Weibiao Cao
Wenqing (Wendy) Cao
Barbara Ann Centeno
Joanna SY Chan
Kung-Chao Chang
Hao Chen
Wei Chen
Yunn-Yi Chen
Sarah Chiang
Soo-Jin Cho
Shefali Chopra
Nicole A. Cipriani
Cecilia Clement
Claudiu Cotta
Jennifer A. Cotter
Sonika M. Dahiya
Elizabeth G. Demicco
Katie Dennis
Jasreman Dhillon
Anand S. Dighe
Bojana Djordjevic
Michelle R. Downes
Charles G. Eberhart
Andrew G. Evans
Fang Fan
Julie C. Fanburg-Smith
Gelareh Farshid
Michael Feely
Susan A. Fineberg
Dennis J. Firchau
Gregory A. Fishbein
Agnes B. Fogo
Andrew L. Folpe
Danielle Fortuna
Billie Fyfe-Kirschner
Zeina Ghorab
Giovanna A. Giannico
Anthony J. Gill
Tamar A. Giorgadze
Alessio Giubellino
Carolyn Glass
Carmen R. Gomez-Fernandez
Shunyou Gong
Purva Gopal
Abha Goyal
Christopher C. Griffith
Ian S. Hagemann
Gillian Leigh Hale
Suntrea TG Hammer
Malini Harigopal
Kammi J. Henriksen
Jonas J. Heymann
Carlo Vincent Hojilla
Aaron R. Huber
Jabed Iqbal
Shilpa Jain
Vickie Y. Jo
Ivy John
Dan Jones
Ridas Juskevicius
Meghan E. Kapp
Nora Katabi
Francesca Khani
Joseph D. Khoury
Benjamin Kipp
Veronica E. Klepeis
Christian A. Kunder
Stefano La Rosa
Stephen M. Lagana
Keith K. Lai
Goo Lee
Michael Lee
Vasiliki Leventaki
Madelyn Lew
Faqian Li
Ying Li
Chieh-Yu Lin
Mikhail Lisovsky
Lesley C. Lomo
Fang-I Lu
aDeqin Ma
Varsha Manucha
Rachel Angelica Mariani
Brock Aaron Martin
David S. McClintock
Anne M. Mills
Richard N. Mitchell
Hiroshi Miyamoto
Kristen E. Muller
Priya Nagarajan
Navneet Narula
Michiya Nishino
Maura O'Neil
Scott Roland Owens
Burcin Pehlivanoglu
Deniz Peker Barclift
Avani Anil Pendse
Andre Pinto
Susan Prendeville
Carlos N. Prieto Granada
Peter Pytel
Stephen S. Raab
Emilian V. Racila
Stanley J. Radio
Santiago Ramon Y Cajal
Kaaren K Reichard
Jordan P. Reynolds
Lisa M. Rooper
Andrew Eric Rosenberg
Ozlen Saglam
Ankur R. Sangoi
Kurt B. Schaberg
Qiuying (Judy) Shi
Wonwoo Shon
Pratibha S. Shukla
Gabriel Sica
Alexa Siddon
Anthony Sisk
Kalliopi P. Siziopikou
Stephanie Lynn Skala
Maxwell L. Smith
Isaac H. Solomon
Wei Song
Simona Stolnicu
Adrian Suarez
Paul E. Swanson
Benjamin Jack Swanson
Sara Szabo
Gary H. Tozbikian
Gulisa Turashvili
Andrew T. Turk
Efsevia Vakiani
Paul VanderLaan
Hanlin L. Wang
Stephen C. Ward
Kevin M. Waters
Jaclyn C. Watkins
Shi Wei
Hannah Y. Wen
Kwun Wah Wen
Kristy Wolniak
Deyin Xing
Ya Xu
Shaofeng N. Yan
Zhaohai Yang
Yunshin Albert Yeh
Huina Zhang
Xuchen Zhang
Bihong Zhao
Lei Zhao

To cite abstracts in this publication, please use the following format: **Author A, Author B, Author C, et al. Abstract title (abs#). In "File Title."** ***Modern Pathology*** **2022; 35 (suppl 2): page#**

1089 Enhanced Clinical Utility of Integrative Whole Genome Sequencing (WGS) and RNAseq Analysis of Primary Brain Tumors

Majd Al Assaad[1], Gunes Gundem[2], Kentaro Ohara[3], Juan Medina-Martínez[2], Jyothi Manohar[3], Michael Sigouros[3], Minal Patel[2], David Wilkes[3], Elli Papaemmanuil[2], David Pisapia[3], Juan Miguel Mosquera[3]
[1]New York-Presbyterian/Weill Cornell Medicine, New York City, NY, [2]New York, NY, [3]Weill Cornell Medicine, New York, NY

Disclosures: Majd Al Assaad: None; Gunes Gundem: *Consultant*, Isabl Technologies; Kentaro Ohara: None; Juan Medina-Martínez: *Stock Ownership*, Isabl Inc.; Jyothi Manohar: None; Michael Sigouros: None; Minal Patel: *Employee*, Isabl Inc.; David Wilkes: None; Elli Papaemmanuil: *Stock Ownership*, Isabl Inc.; David Pisapia: None; Juan Miguel Mosquera: None

Background: Next-generation sequencing (NGS) of tumors reveals diagnostic, prognostic, risk stratifying and targetable mutations. WGS provides the opportunity for new discoveries through analysis of structural variants, non-coding regions, and enhancer hijacking. To unearth known and novel tumor drivers, we employed an integrative WGS/RNAseq analytic platform on a heterogenous group of brain tumors and compared findings with whole exome sequencing (WES) and targeted NGS results.

Design: WGS of matched tumor/normal, and RNAseq data from 28 primary brain tumors were analyzed using Isabl GxT (*BMC Bioinformatics* 2020), a platform that processes NGS from multiple high-throughput sources, uses a relational database to analyze the data and displays it on a web-based user-friendly interface that integrates OncoKB. Structural variants, mutational signatures, SNV, CNA, germline events and expression clustering were interrogated. Data were compared to WES (all 28 cases) and targeted NGS (21 cases).

Results: Diagnoses and age (range 6 to 78 years) are listed in Table 1. Average processing time of integrative WGS/RNAseq Isabl GxT was 10 hours. All cases were MSI stable except for choroid plexus carcinoma (case 28) with MSI score of 6.68 (indeterminate). All clinically relevant findings from targeted NGS and WES were detected by Isabl GxT platform. At least 1 additional targetable and/or clinically relevant alteration was identified in 11 of 28 tumors by WGS/RNAseq. Examples include a duplication event with concurrent overexpression of FGFR1 in a poorly characterized pilocytic astrocytoma (case 26; Figure 1). The platform uncovered targetable mutation signatures including double-stranded break (DSB) repair (cases 1 and 17) in 1 case of 'Astrocytoma, IDH-mutant, Grade 2' and 1 case of 'Glioblastoma, IDH-wildtype, Grade 4'; homologous recombination deficiency (HRD) in 1 case of 'Astrocytoma, IDH-mutant, Grade 4', (case 15) and alkylating agent signature in 1 'Astrocytoma, IDH-mutant, Grade 4' that recurred two years after receiving an alkylating agent (case 27; Figure 2).

Table 1: Patients' characteristics and notable genomic events.

ID	diagnosis	Age	Onco KB	Signatures	Gene	Type of event
1	Astrocytoma, IDH-mutant	32	1	DSB repair	-	-
2	Glioblastoma, IDH wildtype	76	4	aging	CHEK1*	copy number alteration
3	Glioblastoma, IDH wildtype	64	3	aging	-	-
4	High grade neuroepithelial neoplasm, NOS	6	0	aging	-	-
5	Glioblastoma, IDH wildtype	41	5	aging	EGFR*	inversion duplication and deletion
6	Glioblastoma, IDH wildtype	59	8	aging	-	-
7	Glioblastoma, IDH wildtype	71	0	aging	-	-
8	Glioblastoma, IDH wildtype	9	6	aging	-	-
9	Glioblastoma, IDH wildtype	60	2	aging	-	-
10	Glioblastoma, IDH wildtype	58	5	aging	NF1, PIK3R1**	Stop gained, inframe variant
11	Glioblastoma, IDH wildtype	72	4	aging	PDGFRA^	Non-synonymous codon SNV
12	Glioblastoma, IDH wildtype	77	4	aging	-	-
13	Astrocytoma, IDH-mutant	46	1	unknown	-	-
14	Glioblastoma, IDH wildtype	62	6	aging	PTEN^	Non-synonymous codon SNV

15	Astrocytoma, IDH-mutant	30	1	Homologous recombination deficiency	-	-
16	Glioblastoma, IDH wildtype	78	9	aging	-	-
17	Glioblastoma, IDH wildtype	42	6	DSB repair	-	-
18	Glioblastoma, IDH wildtype	74	0	aging	-	-
19	Glioblastoma, IDH wildtype	70	9	aging	BRCA2^	Deletion
20	Glioblastoma, IDH wildtype	61	2	aging	-	-
21	Glioblastoma, IDH wildtype	69	4	aging	NF1, MET*	Frameshift variant
22	Glioblastoma, IDH wildtype	78	5	aging	PTEN**	Frameshift variant
23	Glioblastoma, IDH wildtype	67	2	aging	PTEN**	Stop gained
24	Glioblastoma, IDH wildtype	53	4	aging	-	-
25	Glioblastoma, IDH wildtype	45	6	aging	PTEN^	Frameshift variant
26	pilocytic astrocytoma	15	0	aging	FGFR1^	duplication involving exons 9-18
27	Astrocytoma, IDH-mutant	34	9	Alkylating agent	-	-
28	choroid plexus carcinoma	18	0	aging	-	-

*Genomic lesion detected on combined analysis only- NGS not done

**Genomic lesion detected on combined analysis and targeted NGS but not on RNAseq

^Genomic lesion detected on combined analysis but not detected on targeted analysis nor on RNAseq

-= No available NGS results

Figure 1 - 1089

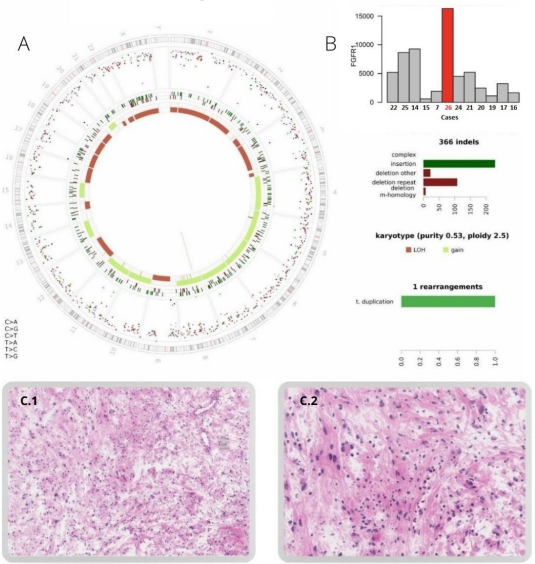

Figure 1. Case 26, pilocytic astrocytoma. No targets were detected by WES or targeted NGS.
A. Circos plot with duplication event in chr. 8p involving FGFR1.
B. Overexpression (RNAseq) of FGFR1
C. Histopathology (H&E, 10x and 20x original magnification)

Figure 2 - 1089

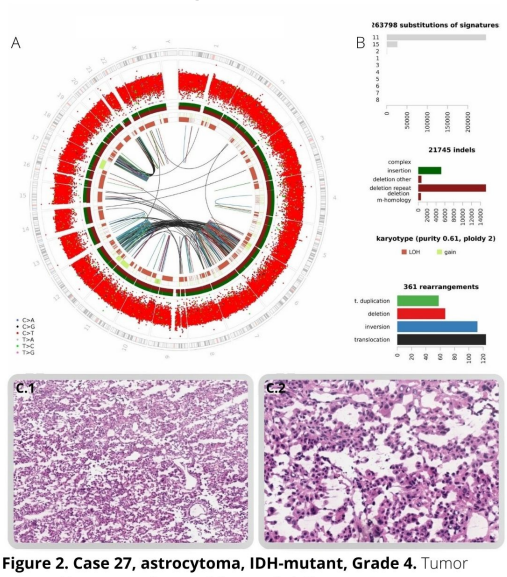

Figure 2. Case 27, astrocytoma, IDH-mutant, Grade 4. Tumor recurred two years after receiving an alkylating agent.
A. Circos plot with mutiple rearrangements. Tumor harbored 3162 SNVs and 101 indels.
B. Molecular signatures included alkylating agent.
C. Histopathology (H&E, 10x and 20x original magnification)

Conclusions: This pilot study demonstrates that integrative WGS/RNAseq enhances the detection of clinically relevant genomic alterations and potential targets that are not readily identifiable through other NGS technologies. It will have significant impact, e.g. clinical trials are testing DNA damage response inhibitors in glioblastoma and correlating DNA repair defects with sensitivity to specific DDR inhibitors can help patient selection.

1090 The Spectrum of Lipid Storage Myopathy in Indian Population : A Correlative Study of Muscle Biopsy with Tandem Mass Spectrometric Analysis of Blood Carnitines - A retrospective survey of two decades (2000-2020)

Nivetha Ambalavanan[1], Rita Christopher[2], Gayathri Narayanappa[2], Nandeesh B N[2], Yasha Chikkabasavaiah[2]
[1]All India Institute of Medical Sciences, New Delhi, India, [2]Bengaluru, India

Disclosures: Nivetha Ambalavanan: None; Rita Christopher: None; Gayathri Narayanappa: None; Nandeesh B N: None; Yasha Chikkabasavaiah: None

Background: Lipid storage myopathy (LSM) is one of the rare causes of inborn errors of metabolism presenting with primary myopathy. Skeletal muscle biopsy reveals vacuoles with prominent lipid droplets in these disorders like primary carnitine deficiency(PCD), multiple acyl-coenzyme-A dehydrogenase deficiency(MADD), and neutral lipid storage diseases(NLSDs), whereas subtle changes with minimal lipid accumulation are seen in intramitochondrial lipid metabolism dysfunction like Very long-chain acyl CoA dehydrogenase deficiency (VLCAD), Carnitine palmitoyltransferase II deficiency (CPTII) and Mitochondrial trifunctional protein deficiency (MTP deficiency). Tandem mass spectrometric (TMS) analysis of a panel of carnitines in the blood by Dried blood spot (DBS) is a less invasive and quick initial screening test for diagnosis and characterization of lipid dysmetabolism. This study establishes to correlate and integrate histomorphology with biochemical abnormalities in these disorders.

Design: To analyze the spectrum of Lipid storage myopathies in the Indian population from a tertiary care neuro center with Tandem mass spectrometric analysis of a panel of blood carnitines. Cases diagnosed as Lipid storage myopathy in muscle biopsies between the years 2000 to 2020 were included in the study and corresponding carnitine panel analysis in blood was evaluated and correlated with relevant clinical history.

Results: Over a span of 21 years, there were 35 diagnosed cases of Lipid storage myopathies based on histomorphology in muscle biopsies. Of which 32 patients had TMS analysis done in dried blood spots (DBS). Lipid dysmetabolism is noted in 20 cases with abnormal carnitine levels diagnosed as following: 50% (n = 10) had Multiple acyl CoA dehydrogenase deficiency (MADD), 20% (n=4) had Medium-chain acyl CoA dehydrogenase deficiency (MCAD), 15% (n=3) had carnitine deficiency, 10% (n=2) had Very long-chain acyl CoA dehydrogenase deficiency (VLCAD) and 1 case of Carnitine acylcarnitine translocase deficiency (CACT). 12 cases did not show any particular abnormality.

Frequency of fatty oxidation defect - Based on Tandem Mass Spectrometric analysis of a panel of Carnitines

S.No	Subtype	number of cases	Percentage
1	Multiple acyl CoA dehydrogenase deficiency	10	50%
2	Medium-chain acyl CoA dehydrogenase deficiency	4	20%
3	Carnitine deficiency (Primary or Secondary)	3	15%
4	Very long-chain acyl CoA dehydrogenase deficiency (VLCAD)	2	10%
5	Carnitine acylcarnitine translocase deficiency	1	5%
	Total	20	

Figure 1 - 1090

Carnitine panel	Reference	Patient Profile
Free carnitine, C0	9 - 65	16.31
Acetylcarnitine, C2	2.8 - 45	14.34
Propionylcarnitine, C3	0.30 - 5.81	0.74
Malonylcarnitine, C3DC	0.00 - 0.68	0.18
Butyrylcarnitine, C4	0.06 - 1.14	0.37
Methylmalonylcarnitine, C4DC	0.00 - 2.60	0.21
3-OH-butyrylcarnitine, C4-OH	0.04 - 0.94	0.18
Isovaleryl/2-methylbutyrylcarnitine, C5	0.03 - 0.65	0.3
Tiglylcarnitine, C5:1	0.00 - 0.11	0
3-OH-isovalerylcarnitine, C5-OH	0.03 - 0.67	0.21
Glutarylcarnitine, C5-DC	0.00 - 0.41	0.11
Hexanoylcarnitine, C6	0.00 - 0.40	0.38
Adipylcarnitine, C6DC	0.00 - 0.50	0.03
Octanoylcarnitine, C8	0.01 - 0.39	0.61 *
Octenoylcarnitine, C8:1	0.01 - 0.87	0.03
Decanoylcarnitine, C10	0.00 - 0.45	1.23 *
Decenoylcarnitine, C10:1	0.01 - 0.30	0.13
Dodecadienoylcarnitine, C10:2	0.00 - 0.17	0.01
Dodecanoylcarnitine, C12	0.02 - 0.42	0.83 *
Dodecenoylcarnitine, C12:1	0.01 - 0.39	0.15
Tetradecanoylcarnitine, C14	0.03 - 0.41	0.78 *
Tetradecenoylcarnitine, C14:1	0.01 - 0.28	0.8 *
3-OH-tetradecenoylcarnitine, C14-OH	0.01 - 0.08	0 *
Hexadecenoylcarnitine, C16	0.74 - 6.46	2.02
Hexadecenoylcarnitine, C16:1	0.02 - 0.66	0.91 *
3-OH-hexadecanoylcarnitine, C16-OH	0.01 - 0.17	0.01
Stearoylcarnitine, C18	0.29 - 1.8	0.9
Oleylcarnitine, C18:1	0.34 - 2.4	1.93
Linoleylcarnitine, C18:2	0.02 - 1.21	0.75
3-OH-octdecanoylcarnitine, C18-OH	0.01 - 0.13	0 *
3-OH-oleylcarnitine, C18:1-OH	0.01 - 0.20	0.02

Figure 2 - 1090

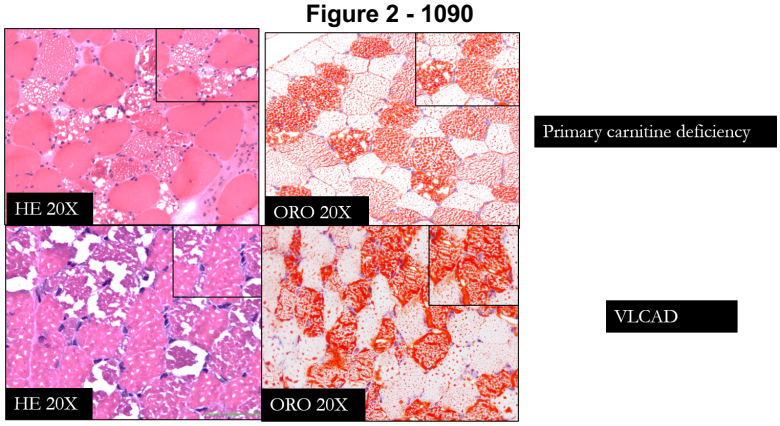

Conclusions: Multiple acyl Co-A dehydrogenase deficiency is the most frequently diagnosed lipid storage disorder in the Indian population presenting with primary myopathies. Dried blood spot (DBS) for analysis of Carnitine profile plays a crucial role as a screening tool in diagnosis. Diagnosis of muscle biopsy should be accompanied by a DBS-TMS panel of carnitines for accurate characterization of storage disorders for an early therapy in patients.

1091 Primary Diffuse Large B-cell Lymphoma of the Central Nervous System: Unmet Medical Need

Sofia Asioli[1], Claudio Agostinelli[2], Luca Morandi[1], Matteo Zoli[3], Diego Mazzatenta[3], Marica Iommi[1], Simona Righi[1], Elena Sabattini[4], Pier Luigi Zinzani[1], Alessandro Broccoli[4], Ginmarco Bagnato[4], Luigi Cirillo[3], Caterina Tonon[3], Raffaele Lodi[3], Caterina Giannini[5]

[1]University of Bologna, Bologna, Italy, [2]IRCCS Azienda Ospedaliero-Universitaria di Bologna, Bologna, Italy, [3]IRCCS Istituto delle Scienze Neurologiche di Bologna, Bologna, Italy, [4]Sant'Orsola-Malpighi Academic Hospital of Bologna, Italy, Bologna, Italy, [5]Mayo Clinic, Rochester, MN

Disclosures: Sofia Asioli: None; Claudio Agostinelli: None; Luca Morandi: None; Matteo Zoli: None; Diego Mazzatenta: None; Marica Iommi: None; Simona Righi: None; Elena Sabattini: None; Pier Luigi Zinzani: *Advisory Board Member*, Secura Bio, Celltrion, Gilead, Janssen-Cilag, BMS, Servier, Sandoz, MSD, TG Therap, Takeda, Roche, Eusapharma, Kyowa Kirin, Novartis, ADC Therap, Incyte, Beigene; Alessandro Broccoli: None; Ginmarco Bagnato: None; Luigi Cirillo: None; Caterina Tonon: None; Raffaele Lodi: None; Caterina Giannini: None

Background: Primary diffuse large B-cell lymphoma of the CNS (PCNSL) is an aggressive disease, with dismal prognosis despite the use of high dose methotrexate (MTX)-based polychemotherapy. New therapeutic approaches are needed to improve patient survival. Our study aims to assess the biologic profiles of PCNSL and to correlate them with clinical/imaging findings to gain diagnostic insight into PCNSL and possibly identify new therapeutic targets.

Design: We studied 57 PCNSL patients, mean age 64 years (34 – 82), 30 (52,6%) female and 27 male (47,4%) seen at our institution between (2005-2020)**.** PCNSL FFPE samples at first diagnosis were characterized by immunohistochemistry including CD20, CD10, BCL2 (cut-off 50%), BCL6, IRF4 and cMYC (cut-off 40%). *cMYC* rearrangements were evaluated by fluorescence in situ hybridization and PCNSL recurrently mutated genes were evaluated by Next Generation Sequencing. The biologic profiles were correlated to available imaging and clinical data.

Results: All 57 PCNSL were positive for CD20, 10 (17.5%) for CD10, 47 (82.4%) for BCL2, 48 (84.2%) for BCL6, 53 (of 56;94.6%) for IRF4 and 38 (of 56;67.8%) for cMYC. BCL2/cMYC double expression was present in 33 (of 57; 57.9%). *cMYC* gene rearrangement was detected in 2 (of 56;3.6%) cases, associated with *BCL6* translocation (double-hit MYC^{t}/BCL6^{t}) only in 1 case. We found mutation of *PIM1* in 22 (of 36;61,1%) cases, *MYD88* in 22 (of 37;59,5%), *CD79B* in 11 (of 36;30,6%), *Notch1* in 6 (of 29;20,7%) and *TP53* in 6 (of 31;19,4%).

PCNSLs patients with a solitary lesion carried MYD88 L265P mutation more commonly than those with multiple lesions [14 (of 18) single lesion vs. 8 (of 19) with multiple lesions; p 0.045]. *MYD88* L265P mutation was significantly associated with a higher overall response rate to chemotherapy (MTX+cytarabine or MATRix regimen) [5 (of 6) responder in MYD88^{mut} patients vs 0 (of 5) in MYD88^{wt}; p=0.015].

Conclusions: As previously reported, PCNSLs frequently show double expression of BCL2/cMYC proteins, but only rarely carry *cMYC* rearrangements. *MYD88*, *PIM1* and *CD79B* are the most recurrently mutated genes. *MYD88* mutated PCNSLs present more frequently as a solitary lesion and may respond better to chemotherapy.

1092 Evaluation of WNT-Pathway Immunohistochemical Stains for Molecular Subtypes of Medulloblastoma and the Utility of H-Score Thresholds

Nicole Becker[1], Karra Jones[2], Andrew Bellizzi[1]
[1]University of Iowa Hospitals & Clinics, Iowa City, IA, [2]The University of Iowa, Iowa City, IA

Disclosures: Nicole Becker: None; Karra Jones: None; Andrew Bellizzi: None

Background: Medulloblastomas are divided into molecular subtypes (WNT, SHH, or non-WNT/non-SHH). A panel of immunohistochemical (IHC) stains including GAB1, YAP1, and beta-catenin have been suggested to identify each subtype. YAP1 and nuclear beta-catenin positivity are used to identify WNT-pathway tumors yet have challenges in interpretation, including focal nuclear staining and lab-to-lab variability. LEF1, glutamine synthetase (GS), cyclin D1, and c-Myc are WNT-pathway activation surrogates used in other organ systems. We set out to validate GAB1 and YAP1 in our laboratory and explore other IHC markers of WNT-pathway activation that might be useful in medulloblastoma molecular subtyping.

Design: Medulloblastomas were identified and given a morphologic classification. Tissue microarrays (TMAs) were created (n=80; triplicate 1.5 mm cores) for cases with sufficient tissue to array or stained as whole sections (n=2). Molecular testing results were available for 21 cases (SHH=6, WNT=1, non-WNT/non-SHH=8, inconclusive=6). IHC stains for GAB1, YAP1, beta-catenin, LEF1, GS, cyclin D1, and c-Myc were performed. H-scores were calculated for GAB1, YAP1, LEF1, GS, cyclin D1, and c-Myc. Beta-catenin was evaluated by stain distribution (membranous, cytoplasmic, or nuclear). GAB1 (H-score >/=200) and YAP1 (>/=150) were thresholded based on cases with available molecular data to infer SHH (GAB1+, YAP1+), WNT (GAB1-, YAP1+), and non-WNT/non-SHH (GAB1-, YAP1-) subtypes for the entire cohort. Statistical analyses were performed for WNT surrogate markers using Fisher's exact test with significance set at a p-value <0.05.

Results: We analyzed the staining of 82 medulloblastomas which were classified as WNT (4%, n=3), SHH (28%, n=23), and non-WNT/non-SHH (68%, n=56). SHH tumors (assigned based on GAB1 >/=200) had variable YAP1 staining (H-score range: 0-150). Beta-catenin demonstrated no nuclear staining in any tumors, even in the confirmed WNT case. Of the WNT surrogate markers, LEF1 was the most frequently expressed in WNT vs non-WNT tumors (p<0.05). See the Table for results of additional IHC stains.

Inferred Molecular Subtype	Morphologic Classification	Mean H-score (median; range)					
		GAB1	YAP1	LEF1	GS	Cyclin D1	c-Myc
WNT	C (3)	43 (0; 0-130)	193 (175; 165-240)	193 (280; 0-300)	168 (215; 43-245)	0 (0; 0-0)	75 (95; 0-130)
SHH	C (9) DN (8) LCA (6)	263 (270; 200-300)	81 (80; 0-260)	80 (27; 0-260)	138 (130; 5-300)	8 (0; 0-140)	5 (0; 0-117)
Non-WNT/non-SHH	C (45) DN (2) LCA (9)	25 (0; 0-180)	9 (0; 0-155)	27 (0; 0-300)	110 (98; 0-285)	0 (0; 0-2)	12 (0; 0-82)

Morphology: C = Classic, DN = Desmoplastic/nodular, LCA = Large cell anaplastic

H-score = intensity (0-3+) x percent tumor staining

Conclusions: Utilization of H-score thresholds for GAB1 and YAP1 is important for inferring medulloblastoma molecular subtypes, as GAB1 can have weak staining especially in non-WNT/non-SHH tumors. This study also highlights frequent focal staining for YAP1 and the limited utility of nuclear beta-catenin accumulation. LEF1 is significantly overexpressed in WNT-pathway activated tumors and deserves further attention as a complement to YAP1 in this diagnostic setting.

1093 Sox2 Expression in Optic Nerve of Retinoblastoma Affected Eyes

Lourdes Cabrera-Muñoz[1], M Veronica Ponce[2], Orjuela Manuela[3], Guillermina Baay[4], Stanislaw Sadowinski-Pine[1]
[1]Hospital Infantil de Mexico Federico Gomez, Cuauhtemoc, Mexico, [2]CMN SXXI, Hospital de Pediatría IMSS, Mexico City, Mexico, [3]Columbia University, New York, NY, [4]Hospital Infantil de Mexico Federico Gomez, Mexico City, Mexico

Disclosures: Lourdes Cabrera-Muñoz: None; M Veronica Ponce: None; Orjuela Manuela: None; Guillermina Baay: None; Stanislaw Sadowinski-Pine: None

Background: Retinoblastoma (RB) is the most frequent intraocular malignant tumor in early childhood; an increase in tumor cells expressing the neural stem cell Marker Sox2 has been associated with invasive RB in enucleated eyes; however there is little information about the expression of Sox2 in optic nerves in patients with RB. The aim of this study is to investigate the expression of Sox2 in optic nerve and RB tissues in enucleated eyes from patient with RB.

Design: 12 Enucleated eyes of patients with retinoblastoma were included; 6 with histopathologic high-risk features (HRF) invasive retinoblastoma (Choroidal infiltration > 3mm and/or post laminar infiltration) and 6 with non-HRF according to the International Retinoblastoma Staging Group. Eyes were processed for routine histopathologic examination; HE Pupil-optic nerve sections including central part of the longitudinally sectioned optic nerve with prelaminar, laminar and retrolaminar portions and a transverse section of the optic nerve surgical margin from each case were reviewed. IHC for Sox2, Vimentin (VIM), glial fibrillary acidic protein (GFAP) and Ki67 was performed in consecutive whole pupil-optic nerve sections in all cases. Qualitative expression of the cell markers (IHC score) was assessed as follows 0+ no expression, 1+, 25%-50% 2+, 50-75 % and 3,+ >75% of tissue.

Results: We found a diffuse pattern of Sox 2 expression in all retrolaminar optic nerve portion in invasive and non-invasive RB. Most of the Sox2+ cells were histologically glial cells and shows IHC co-expression of VIM and GFAP consistent with reactive astrocytes. Higher expression of Sox2 was seen in HRF than in non-HRF RB and in both was associated with intraocular RB necrosis; rare Sox2 positive retinoblastoma cells were present in post laminar infiltration.

Conclusions: This is the first study describing the protein expression of Sox2 in optic nerve glial cells in enucleated eyes with RB; Sox2 expression was associated to both invasive and non-invasive RB and with intraocular RB necrosis in this series.

Sox 2, VIM and GFAP expression in optic nerve glial cells, suggest that they are reactive astrocytes and probably represent the response to proinflammatory chemokins and cytokines; however, the role of RB tumor cells in this astrocyte reactivity cannot be ruled out, here. Further research is needed to investigate the role of optic nerve astrocytes in RB.

1094 Minimal Change Prion Retinopathy: A Morphometric Comparison of Retinal and Brain Prion Deposits in Creutzfeldt-Jakob Disease

Jihee Choi[1], Chiara De Lillo[1], Vanessa Goodwill[2], Ian Dryden[1], Ana Arcia Franchini[1], Christina Sigurdson[3], Jonathan Lin[4]
[1]Stanford University, Palo Alto, CA, [2]University of California, San Diego, [3]UCSD Medical Center, San Diego, CA, [4]Stanford Hospital, Stanford, CA

Disclosures: Jihee Choi: None; Chiara De Lillo: None; Vanessa Goodwill: None; Ian Dryden: None; Ana Arcia Franchini: None; Christina Sigurdson: None; Jonathan Lin: None

Background: Up to 50% of patients with sporadic Creutzfeldt-Jakob disease (sCJD) develop visual symptoms during the disease course. Transmissible 'scrapie-type' prion (PrP^{Sc}) deposits have also been observed in the retinas of sCJD patients. This raises the possibility that visual changes could arise from retinal damage. However, the histopathology of retinal PrP^{Sc} deposits in sCJD is poorly characterized. To investigate this, we performed histologic measurements of retinal PrP^{Sc} deposits from 14 clinically documented sCJD cases for comparison to brain PrP^{Sc} deposits.

Design: From July 2015 to July 2017, 28 eyes and 1 brain were collected from 14 patients with neuropathologically-confirmed sCJD (4 males and 10 females; age range: 51-80, mean: 63.0, SD: ±8.96; disease duration: 1.5-27 mo, mean: 10.5, SD: ±8.38) and eyes and brains were also collected from 6 controls (5 males and 1 female; age range: 51-90, mean: 70.3, SD: ±13.84). Genetic analysis of the prion protein gene (PRNP) was performed in sCJD patients. Histology and immunohistochemistry were performed with Mab12F10 (Cayman Chemical; 1:200) against PrP^{Sc} on retinal and brain sections. The greatest dimension of PrP^{Sc} staining was microscopically measured in the retinas and the brain. Statistical significance was evaluated with Mann-Whitney U test, Welch's unpaired *t*-test, and Brown-Forsythe test.

Results: PrP^{Sc} deposits were observed in the retina by immunohistochemistry. PrP^{Sc} was limited to the outer (OPL) and inner plexiform layers (IPL) of the retina with the strongest deposition as discrete, regularly spaced ovoid deposits in a "beads-on-a-string" pattern along the horizontal axis of the OPL. The average size of retinal PrP^{Sc} deposits from the OPL was 4.94 ± 0.47µm, which was significantly smaller than PrP^{Sc} deposits in the brain (32.45 ± 23.55µm, $p<0.001$). No spongiotic changes were observed in the retinas with PrP^{Sc} deposition. Retinal laminar morphology and thickness (which attenuate with retinal degeneration) appeared comparable between sCJD retinas and controls.

Conclusions: Our findings support that retinal histopathology differs from brain neuropathology in sCJD. First, PrP^{Sc} deposits were consistently present in linear expression in the OPL of the retinas. Second, the deposits in the eye were significantly smaller and relatively uniform in size compared to those in the brain, without overt spongiform changes and neuronal loss. We suggest that in vivo retinal imaging of this stereotypic retinal prion pathology may be useful for diagnosis of patients with clinically suspected prion disease.

1095 A Digital Morphometric Comparison of Nucleolar Features in BAP1-Mutant versus BAP1-Wildtype Uveal Melanomas

Ian Dryden[1], Korina Steinbergs[2], Jonathan Lin[3]
[1]Stanford University, Palo Alto, CA, [2]Stanford University, Stanford, CA, [3]Stanford Hospital, Stanford, CA

Disclosures: Ian Dryden: None; Korina Steinbergs: None; Jonathan Lin: None

Background: Uveal melanomas (UM) are the most common primary intraocular malignancy in adults. With use of gene expression profiling (GEP), UMs can be prognostically categorized as either Class 1 (low risk) or Class 2 (high risk) tumors. Most high-risk metastatic UMs harbor a deactivating mutation BRCA1 associated protein-1 (BAP1) gene, a tumor suppressor gene located on chromosome 3p. A BAP1 mutation leads to loss of nuclear BAP1 expression and a dedifferentiated phenotype, which strongly correlates with a high-risk Class 2 GEP. Recent investigations have shown that the digital morphometry of tumor nuclei correlate with BAP-1 status; however, the relationship between BAP1 status and nucleolar features remains to be described.

Design: The BAP1 mutation status of 10 UMs was determined immunohistochemically with use of anti-BAP1 monoclonal antibody (C-4, Santa Cruz Biotechnology, sc-28383) and confirmed molecularly with use of a solid tumor actionable mutation panel. Ten H&E stained slides composed of 5 BAP1-mutant and 5 BAP1-wildtype UMs were scanned via Phillips IntelliSite Scanner and uploaded as whole slide images to the Phillips Intellisite Suite for morphometric analysis. The longest nucleolar diameter (in µm) and the number of nucleolar organizing regions (NORs) was determined for a hundred consecutive tumor nuclei in one high-powered field for a total of 1,000 tumor cells. A Student T-test was performed to determine if a statistical difference existed between the mean nucleolar diameter and the NOR number in the BAP1-mutant versus BAP1-wildtype groups.

Results: The BAP1-mutant group had a mean nucleolar diameter of 2.5 µm (range 1.1–9.1) and mean NOR number of 1.4 (range 1–5). The BAP1-wildtype group had a mean nucleolar diameter of 1.9 µm (range 0.5–4.6) and mean NOR number of 2.3 (range 1–6). A strong statistical difference between mean nucleolar diameter ($p = 1.05E-61$) and the mean NOR number ($p = 1.263E-53$) was observed between BAP1-mutant and BAP1-wildtype UM groups.

Conclusions: BAP1-mutant UMs tend to have larger nucleoli and fewer NORs than BAP1-wildtype UMs. This finding supports previous research regarding the prognostic relevance of nucleolar size and number of NORs in high-risk versus low-risk UMs but suggests that BAP1 alteration may account for these observations. With incorporation of other known BAP1 associated morphometry, use of advanced whole slide image analytical techniques on digitally scanned H&E slides may allow for prediction of BAP1 status and GEP Class.

1096 Neuronal Injury of Cerebellar Dentate Nucleus: Histopathologic Examination and Clinical Correlation

Bilge Dundar[1], Busranur Agac[2], Eyas Alzayadneh[2], Kyle Conway[1]
[1]University of Iowa, Iowa City, IA, [2]University of Iowa Hospitals & Clinics, Iowa City, IA

Disclosures: Bilge Dundar: None; Busranur Agac: None; Eyas Alzayadneh: None; Kyle Conway: None

Background: The dentate nucleus of cerebellum is a known site of toxic and metabolic injury to the brain, including associations with metronidazole exposure and hepatic encephalopathy. Changes resembling acute ischemia are frequently seen, but the clinical significance of these changes remains unexplored.

Design: Adult autopsy cases with dentate nucleus sampling between 2018-2021 were reviewed. Retrospective analysis performed on electronic medical record. Histologic evaluation of the dentate nucleus included measurements of mean neuronal diameter, mean neuronal count (in 5 high power fields of 2,500 μm^2 each), cytoplasmic eosinophilia, pyknosis, the presence of Alzheimer's type 2 astrocytes, and the presence of autolytic changes in the cerebellar folia. We used multivariate linear regression, controlling for the presence of autolytic changes, to evaluate the relationship between neuronal changes and clinical and pathologic parameters.

Results: We identified 52 cases meeting our inclusion criteria. The mean neuron diameter was 19 microns (± 3.7 microns). Commonly observed pathologic changes included cytoplasmic eosinophilia (46%), Alzheimer's type 2 astrocytes (35%), and pyknosis (35%) (Fig. 1). A decrease in mean neuron diameter was strongly associated with Alzheimer's type 2 astrocytes, cytoplasmic eosinophilia, nuclear pyknosis, and the presence of autolytic changes (Table 1). After controlling for the presence of autolytic changes, several clinical parameters were associated with a decrease in mean neuron diameter: active liver disease (β=-3.7, $p < 0.01$), recent metronidazole exposure (β=-2.6, $p = 0.025$), and history of diabetes mellitus ($p = 0.02$).

Table 1. Clinical and pathologic associations with mean dentate neuron diameter

	All patients		Association with neuron diameter		
	n =	52	beta	95% CI	
Baseline characteristics					
Age, yrs, +/- SD	64.7	± 16.6	**0.7**	**(0.02 to 0.13)**	*
Male, n (%)	33	(63)	1.0	(-0.9 to 2.9)	
Dentate pathology					
Neuron density (per 5 HPF), ± SD	64.7	± 16.6	0.02	(-0.27 to 0.23)	
Alzheimer's type 2 astrocytes, n (%)	18	(35)	**-4.9**	**(-6.6 to -3.2)**	*
Cytoplasmic eosinophilia, n (%)	24	(46)	**-4.5**	**(-5.2 to -2.0)**	*
Nuclear pyknosis, n (%)	18	(35)	**-6.8**	**(-6.6 to -3.6)**	*
Autolytic changes, n (%)	33	(63)	**-3.7**	**(-5.6 to -1.7)**	*
Active systemic disease at death					
Liver disease, n (%)	12	(23)	**-3.7**	**(-5.7 to -1.6)**	*
Acute kidney injury, n (%)	21	(40)	-0.6	(-2.5 to 1.3)	
Pulmonary disease, n (%)	33	(63)	-1.0	(-2.9 to 0.8)	
Recent medicine exposure					
Metronidazole, n (%)	9	(17)	**-2.6**	**(-0.35 to -4.9)**	**
Vascular disease					
Cerebellar arteriosclerosis, (1-3), ± SD	1.4	± 0.9	0.5	(-0.5 to 1.5)	
Heart weight, g, ± SD	460	± 153	0.0	(-0.0 to 0.0)	
History of hypertension, n (%)	36	(69)	-1.8	(-3.8 to 0.2)	
History of diabetes, n (%)	16	(31)	**-2.4**	**(-4.3 to -0.4)**	**
Other neuropathology					
Hypoxic-ischemic injury, n (%)	8	(15)	-1.2	(-3.7 to 1.4)	
Neurodegenerative disease, n (%)	22	(42)	1.0	(-0.9 to 2.9)	

* p-value < 0.01 ** p-value < 0.05

Figure 1 - 1096

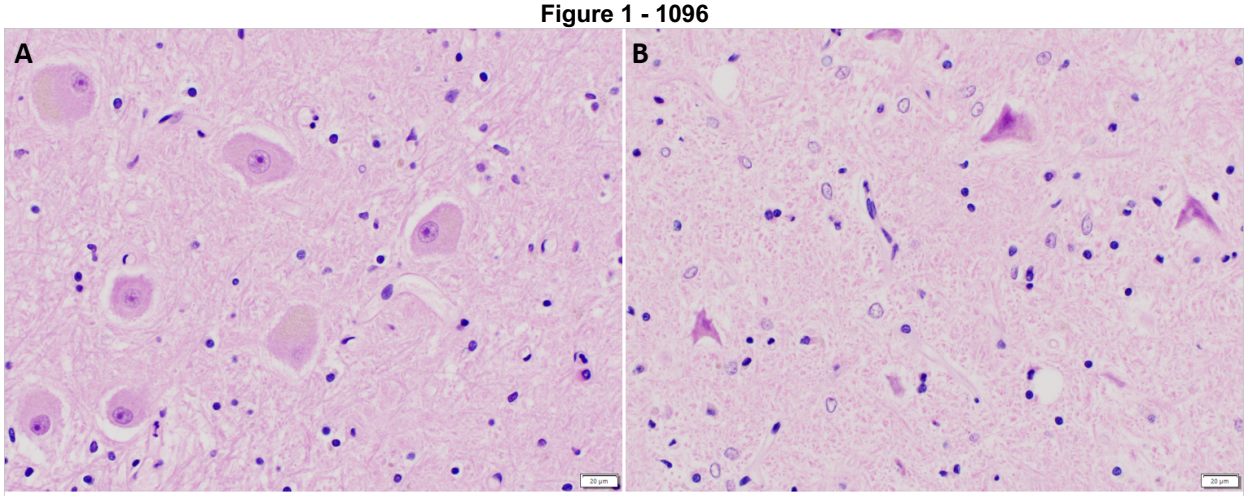

Figure 1. Characteristic pathologic changes to the dentate nucleus. (A) The typical dentate nucleus is composed of neurons with a neuron-body diameter of greater than 20 microns, a large, prominent nucleolus, and amphophilic cytoplasm. The background is composed of quiescent astrocytes and oligodendrocytes. (B) When subject to a variety of metabolic injuries, the neuron-body diameter decreases, the nucleus takes on a pyknotic appearance with loss of the prominent nucleolus, and the cytoplasmic becomes more prominently eosinophilic. Astrocytes with large, irregularly shaped and cleared-out nuclei may be variably prominent.

Conclusions: In this hospital-autopsy based cohort of decedent, pathologic changes to the dentate nucleus were common. The diameter of neuronal cell bodies is the overall best indicator of injury to the dentate. The clinical parameters most strongly associated with a reduction in mean neuron diameter are those related to toxic/metabolic injury, with the presence of liver disease being the strongest association. Further areas of investigation include detailed investigation of laboratory values associated with dentate injury and clinico-radiologic correlations.

1097 Molecular and Clinicopathologic Characterization of Post-Transplant Lymphoproliferative Disorder (PTLD) Involving the Central Nervous System

Ekin Guney[1], Calixto-Hope Lucas[1], Sanda Alexandrescu[2], Bret Mobley[3], Serguei Bannykh[4], Suzanne Powell[5], Angus Toland[6], Hannes Vogel, Christian Davidson[7], Kristian Schafernak[8], Janna Neltner[9], Daniel Boue'[10], Eyas Hattab[11], Sean Ferris[12], Robert Ohgami[1], Melike Pekmezci[1], Andrew Bollen[1], Tarik Tihan[1], Arie Perry[1], David Solomon[1], Kwun Wah Wen[1]
[1]University of California, San Francisco, San Francisco, CA, [2]Boston Children's Hospital, Harvard Medical School, Boston, MA, [3]Vanderbilt University Medical Center, Nashville, TN, [4]Cedars-Sinai Medical Center, Los Angeles, CA, [5]The Methodist Hospital, Houston, TX, [6]Stanford Health Care, Stanford, CA, [7]University of Utah Health, Salt Lake City, UT, [8]Phoenix Children's Hospital, Phoenix, AZ, [9]University of Kentucky, Lexington, KY, [10]Nationwide Children's Hospital - The Ohio State University, Columbus, OH, [11]University of Louisville, Louisville, KY, [12]University of Michigan Medical School, Ann Arbor, MI

Disclosures: Ekin Guney: None; Calixto-Hope Lucas: None; Sanda Alexandrescu: None; Bret Mobley: None; Serguei Bannykh: None; Suzanne Powell: None; Angus Toland: None; Hannes Vogel: None; Christian Davidson: None; Kristian Schafernak: None; Janna Neltner: None; Daniel Boue': None; Eyas Hattab: None; Sean Ferris: None; Robert Ohgami: None; Melike Pekmezci: None; Andrew Bollen: None; Tarik Tihan: None; Arie Perry: None; David Solomon: None; Kwun Wah Wen: None

Background: Central nervous system (CNS) involvement by post-transplant lymphoproliferative disorder (PTLD) is a rare complication of solid organ and hematopoietic stem cell transplantation. PTLDs are frequently associated with EBV infection and they span a wide morphologic spectrum, from reactive hyperplasia (nondestructive) to identical resemblance to lymphomas (as seen in monomorphic type (M-PTLD)). Polymorphic PTLD (P-PTLD) forms are destructive but do not fulfill strict criteria for malignant lymphomas. PTLD with CNS involvement is not well characterized at the molecular level.

Design: The clinicopathologic features of 25 PTLD (19 M-PTLD and 6 P-PTLD) were retrospectively reviewed. Capture-based next-generation sequencing targeting the coding regions of ~500 cancer-associated genes and select introns was performed on formalin-fixed paraffin embedded tissue from 14 cases (12 M-PTLD and 2 P-PTLD) with sufficient tissue.

Results: Twenty-two patients received solid organ transplants (kidney with n=14, liver with n=8) and 3 had bone marrow transplants. Twenty-three patients had isolated CNS PTLD lesions and 2 had additional gastrointestinal involvement. Disease was predominantly multifocal (58%) with supratentorial (100%) and rare infratentorial (8%) involvement. 4 patients (25%) were treated

with chemoradiotherapy and 16 (75%) were treated with chemotherapy only. Pathologically, all 19 M-PTLD cases showed large B-cell lymphoma (LBCL) morphology. Seventeen of 19 M-PTLD cases (89%) were EBV-positive, whereas all P-PTLD cases were EBV-positive. Five of 12 M-PTLDs (42%) showed either chromosomal copy number gains/losses or known oncogenic alterations including MAP kinase pathway alterations (e.g. *HRAS*, *NRAS*, and *NF1* mutations) and also those frequently occurring in primary CNS lymphoma (e.g. *MYD88*, *CD79B*, *KMT2D* mutations). The 2 P-PTLD cases lacked detected chromosomal copy number changes and oncogenic alterations. The association of molecular alterations and outcome is currently under investigation.

Conclusions: A significant subset of M-PTLD cases (42%) had chromosomal gains/losses or known oncogenic molecular alterations, indicating a clonal/neoplastic process. We are currently investigating the clinicopathologic correlates of clonal genetic alterations in PTLD with involvement of the CNS.

1098 Infant-Type Hemispheric Glioma: New Molecular Alterations and Precision-Medicine Treatment

Wan-Ming Hu[1], Li Yuan[2], Jing Zeng[1]
[1]Sun Yat-sen University Cancer Center, Guangzhou, China, [2]Guangzhou Women and Children's Medical Centre, Guangzhou, China

Disclosures: Wan-Ming Hu: None; Li Yuan: None; Jing Zeng: None

Background: Infant-type hemispheric glioma, harboring alterations in the receptor tyrosine kinases ALK, ROS1, NTRK and MET, is a new subtype of Pediatric-type diffuse high-grade gliomas in the 2021 WHO classification of CNS tumors. It has important clinical therapeutic value with specialized therapeutic drugs. Here, we presented 3 cases of infant-type hemispheric glioma. Patient1 with EML4-ALK fusion which often appeared in lung cancer, the other 2 patients have new molecular alterations which has not been reported before (Patient2 has both NTRK1-TP53/TP53-NTRK1 fusions and p53 protein showed characteristic cytoplasm positive; Patient3 presented a brand-new ALK-QKI fusion combined with ALK mutation and focal SMARCB1 deletion. All these 3 cases received corresponding targeted therapy and have a good recovery and normal neurologic function till now.

Design: Immunohistochemistry

Fluorescent in situ hybridization

Nucleic acid extraction

Whole-transcriptome sequencing

Results: Case 1: (Figure 1.A)

8 months, male, right semiovale center occupation.

Histopathology: High-grade neuroepithelial neoplasm.

IHC: GFAP(only few cells+), Olig2(-), S100(+), CD56(+), Syn(-), NSE(focal+), NeuN(-), CD34(-), INI-1(+), Ki67(10%+).

Characteristic Molecular Information: EML4-ALK fusion.

Follow-up: 15 months, alive.

Case 2: (Figure 1.B)

3 years, female, insular lobe occupation.

Histopathology: Gliosarcoma.

IHC: GFAP(partly+), Olig2(partly+), Vimentin(+), P53(cytoplasm+), pan-TRK(+), Ki67(25%+).

Reticular fiber staining showed biphasic tissue pattern with reticulin-rich sarcomatous and reticulin-free gliomatous elements.

Characteristic Molecular Information: NTRK1-TP53 and TP53-NRTK1 fusion.

Follow-up: 27 months, alive.

Case 3: (Figure 1.C and Table 1)

3 years, male, left parietal occipital lobe occupation.

Histopathology: GBM and AT/RT.

IHC: GFAP(partly+), Olig2(partly+), INI-1(partly-), BRG1(+), SYN(-), CD34(-), BRAF(-), S100(-), CK(-), H3K27M(-), IDH1(-), P53(40%+), ATRX(+), pan-TRK(-), ALK(+), Ki67(30%+).

Characteristic Molecular Information: ALK mutation, ALK-QKI fusion, RAD51C mutation and focal SMARCB1(INI-1) deletion.

Follow-up: 14 months, alive.

No.	INI1-deletion region	INI1-retained region
Germline Mutation	RAD51C p.E218Vfs*33	RAD51C p.E218Vfs*33
Somatic Mutation	SMARCB1 p.R158* abundance 94.5%	
	QKI(Exon1-6)-ALK(Exon20-29) abundance 34.69%	QKI(Exon1-6)-ALK(Exon20-29) abundance 42.94%
	ALK(Exon1-19)-LOC102724152(Intergenic) abundance 29.56%	ALK(Exon1-19)-LOC102724152(Intergenic) abundance 35.27%
	ALK p.A1015T abundance 48.39%	ALK p.A1015T abundance 27.56%
Chromosome Variation	Chromosome 22 deletion	1q21.3-q31.3 amplification CN：2.77

Figure 1 - 1098

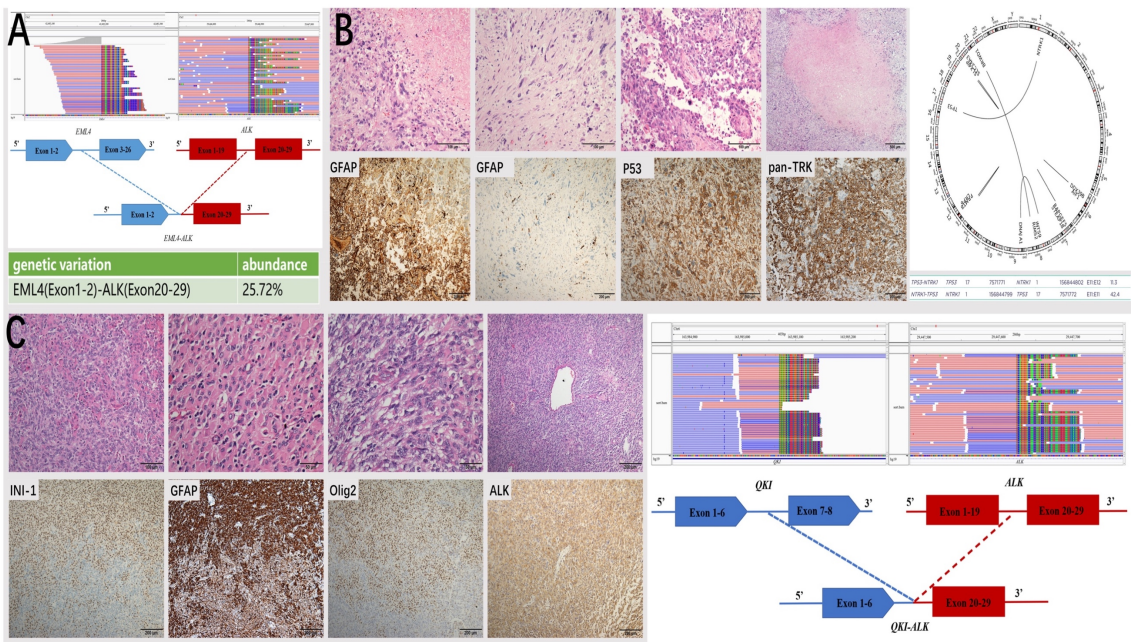

Conclusions: Infant-type hemispheric glioma is a special kind of glioma, which is particularly suitable for precision-medicine treatment approaches. Their overall survival is good compared with other three pHGG subtype.

1099 cfDNA Quantification and IDH1R132H Mutation Detection in Adult Diffuse Glioma on Chemoradiation

Nuzhat Husain[1], Adil Husain[1], Sridhar Mishra[1], Rahat Hadi[1], Rohini Khurana[1]
[1]Dr Ram Manohar Lohia Institute of Medical Sciences, Lucknow, India

Disclosures: Nuzhat Husain: None; Adil Husain: None; Sridhar Mishra: None; Rahat Hadi: None; Rohini Khurana: None

Background: Cell-free DNA (cfDNA) may be a promising biomarker for the diagnosis and categorization of adult diffuse glioma (ADG). Serial cfDNA quantification over the course of chemoradiation may provide a kinetic measure of changes and help predict response to therapy. IDH mutations are critical to distinguishing a wild type glioblastoma and mutant astrocytoma and oligodendroglioma. The current study investigates the change over time in cfDNA in ADGs undergoing chemo-radiotherapy and evaluates detection of $IDH1^{R132H}$ mutation in cfDNA.

Design: The study group comprised histologically confirmed ADGs (n=30), including gliomas of grade II (n=07), III (n=06), and IV (n=17), and controls (n=25). Serum cfDNA was extracted using the ChargeSwitch gDNA 1mL Serum Kit (Invitrogen, USA) and quantified using the β-globin gene. CAST PCR assay (TaqMan® Mutation Detection Assay #4371353, #Hs00000981_mu, #Hs00001019_rf) was performed in cfDNA (n=30) and corresponding FFPE DNA.

Results: Pre-radiotherapy cfDNA levels were higher in patients with ADG (Median; 103.0 ng/mL) as compared to normal controls (Median; 74.37ng/mL) (p=0.04). Serial quantification showed a decreasing trend with mean (Q1-Q3) values of 103.0(26.23-279.20), 88.27(23.25-156.70) and 75.05 (28.26-208.20) (p 0,04) in pretreatment, 3 week and 6 week samples. Significant higher levels were observed with higher grade and larger size ADG. CfDNA showed a decreasing trend in pretreatment vs. 6 week sample in 35.29% responders and an increasing trend in 15.38% of non-responders. Table 1 details differences in cfDNA values in responders (complete and partial) vs nonresponders (stable and progressive disease). cfDNA level was 2.7 times higher than $IDH1^{R132H}$ nonmutated vs mutated non-responders. In CAST PCR assay, $IDH1^{R132H}$ was detected in cfDNA in 2 cases only as compared to 14/30 cases which were positive in FFPE DNA and by immunohistochemistry.

Table 1: Association of cfDNA levels with clinical parameters in responders and non-responders

Characteristics		N	Pre-Treatment CfDNA Median (Q1-Q3)	p-Value
Type of Excision	GTE **R** **NR**	14 08	52.85(20.01-159.5) 425.0(143.8-964.3)	***0.0029***
	PE/Biopsy **R** **NR**	03 05	66.70(5.401-149.4) 67.67(26.40-1970)	0.5714
Grade	II **R** **NR**	05 02	20.08(8.789-97.66) 247.3(239.0-255.6)	0.0952
	III **R** **NR**	04 02	153.0(96.36-301.7) 49.53(31.40-67.67)	0.1333
	IV **R** **NR**	08 09	46.55(21.29-122.4) 740.8(93.95-1220)	***0.0152***
IDH	Mutated **R** **NR**	07 04	27.00(12.18-78.69) 247.3(110.5-996.8)	0.0727
	Non-Mutated **R** **NR**	09 08	131.9(23.11-162.4) 667.7(51.55-1156)	0.0927
Histologic Type	Astrocytoma Oligodendroglioma Glioblastoma	7 6 17	78.69(12.18-156.6) 153.3(25.27-279.2) 112.0 (26.05-889.8)	0.5022
Response	Responder Non-Responder	17 13	66.70(19.95-153.0) 255.6(71.78-1117)	**0.0052**

R-Responder , NR non responder, GTE gross total excision, PE partial excision

Conclusions: In patients with ADG, pre-radiotherapy cfDNA concentration and IDG mutation status is associated with treatment outcomes. IDH1 mutation detection in cfDNA using cast PCR has a poor sensitivity. NGS may be a better option for specific mutation detection in liquid biopsies.

1100 MMR Expression in Gliomas: Clinicopathological Evaluation, a Tertiary Care Cancer Institute Experience

Ramandeep Kaur, Abhishek Chatterjee, Ayushi Sahay, Vikas Singh, Prakash Shetty, Moiyadi Aliasgar, Tejpal Gupta, Sridhar Epari, Archya Dasgupta, Amitkumar Choudhari, Girish Cinnaswammy
[1]Tata Memorial Hospital, Mumbai, India, [2]Tata Memorial Centre, Mumbai, India

Disclosures: Ramandeep Kaur: *Primary Investigator*, tata memorial hospital; *Primary Investigator*, tata memorial hospital; Abhishek Chatterjee: None; Ayushi Sahay: None; Vikas Singh: None; Prakash Shetty: None; Moiyadi Aliasgar: None; Tejpal Gupta: None; Sridhar Epari: None; Archya Dasgupta: None; Amitkumar Choudhari: None; Girish Cinnaswammy: None

Background: Mismatch repair gene (MLH1, MSH2, MSH6, or PMS2) altered familial syndromes include Lynch syndrome and Constitutional mismatch repair deficiency syndrome (CMMRD). CMMRD predisposes to brain tumors and shows a functional bi-allelic loss in the MMR genes. Lynch syndrome (LS) is associated with colorectal & genitourinary malignancies and shows mono-allelic loss of the same set of genes.

Design: We retrospectively included non-consecutive cases of glial tumors that showed immunohistochemical loss of MMR proteins over the last 7 years and evaluated for clinicopathological features.

Results: Cases (n=76) were analyzed immunohistochemically and a pattern of expression of MMR proteins was noted: Complete loss in both tumor and native cells (CMMRD phenotype,n=19), loss in tumor cells only with retained expression in native cells (LS phenotype, n=5), mosaic expression (n=4) and proficient expression (n=48).

CMMRD phenotype: Age-range: 3- 19 years (median: 8; >18 yrs: 2). Male: female= 1.1:1.Hemispheric (n=18) was the commonest location; one was in the posterior fossa. Café au lait macules (n=13), history of consanguinity (n=8), family history of malignancy (n=9), and other malignancies (n=3) were noted. All showed high-grade glial histology with bizarre giant cells (n=14) and relative undifferentiated morphology (n=8). Predominant (n=16) were p53 positive and 9 had ATRX loss. The combined loss of MLH1 and PMS2 was commonest (n=10) followed by isolated loss of PMS2 (n=6). Five of the16 cases died, while 3 are on supportive therapy.

LS phenotype: Age-range: 8- 44 years (median: 8; >18 yrs:3). Male: female= 3:2. All were hemispheric in location. Café au lait macules (n=1), history of consanguinity (n=1), family history of malignancy (n=2), and other malignancies (n=1) were noted. All showed glial morphology and were high grade on histology, however without giant cells or undifferentiated morphology. All were p53 positive with retained ATRX expression. The combined loss of MSH2 and MSH6 (n=3) followed by combined loss of MLH1, PMS2 (n=2). Two patients on follow-up had stable disease over 16 and 31 months.

Conclusions: MMR protein-deficient glial tumors are commonly high grade; affecting children & young adults. CMMRD is more commonly associated; however, glial tumors are also seen in LS. The histological presence of giant cells is common (supportive for the diagnosis of CMMRD in presence of clinical history). Loss of PMS2 is the commonest pattern in CMMRD cases, while MSH6 in Lynch syndrome cases.

1101 Metastatic Tumors to the Pituitary Gland: a Case Series

Melanie Lang-Orsini[1], Maria Martinez-Lage[1]
[1]Massachusetts General Hospital, Boston, MA

Disclosures: Melanie Lang-Orsini: None; Maria Martinez-Lage: None

Background: Metastatic lesions to the pituitary are rare and account for approximately 1% of all pituitary tumors. Diagnosis can be challenging as not all patients are symptomatic. Uncommonly, pituitary metastasis may be the first presentation of malignant disease. Distinguishing these cases from pituitary adenoma is important, as the management and prognosis differs significantly between these two conditions.

Design: Retrospective autopsy and surgical series of metastatic tumors involving the pituitary gland in a single institution over a 20-year period.

Results: We identified 11 metastatic tumors involving the pituitary gland, in 3 autopsies and 8 surgical specimens. The patients ranged in age from 40 to 73, with a median age of 66. Six of the patients were male (54.5%) and five were female (45.5%). The majority of the patients had a pre-existing diagnosis of malignancy (9; 82.8%), but in two cases (18.2%) pituitary symptoms were the initial presentation of malignant disease. The most common diagnosis was metastatic carcinoma (7; 63.6%), with primary sites including lung, kidney and breast (each 2; 18.2%), and prostate (1; 9.1%). Other diagnoses included metastatic melanoma (2; 18.2%), diffuse large B cell lymphoma (1; 9.1%) and acute myeloid leukemia (1; 9.1%). A co-existing pituitary adenoma was present in two patients (18.2%). 6 patients (54.5%) were symptomatic. In the patients with symptomatic lesions, the most common clinical manifestations were visual symptoms, followed by panhypopituitarism. Most patients were treated with a combination of radiation, chemotherapy, immunotherapy or targeted therapy. The median overall survival from time of diagnosis was 45 months. In three of the patients, the diagnosis was made at autopsy, and survival information was not available for one patient.

	Age	Sex	Presenting Pituitary Symptoms	Primary	Time from Diagnosis to Pituitary Metastasis (years)	Other Metastatic Sites at Diagnosis	Treatment	Survival (months)
Patient 1	73	M	Diplopia, left 6th nerve palsy	Prostate	11	None	Chemotherapy, radiation	57
Patient 2	57	M	Visual loss, headaches	Melanoma	8	None	Immunotherapy	9
Patient 3	51	F	Asymptomatic	Breast	4	Brain	Chemotherapy, radiation, targeted therapy	Unknown
Patient 4	51	M	Diabetes insipidus	Lung	Same time	Lymph nodes, liver, adrenal, spleen, bone	Chemotherapy, radiation, immunotherapy	45
Patient 5	66	M	Diplopia	Melanoma	11	None	Radiation, immunotherapy	36
Patient 6	40	F	Panhypopituitarism	Breast	4	None	Chemotherapy, radiation, targeted therapy	48
Patient 7	71	F	Panhypopituitarism	Lung	Same time	None	Radiation	48
Patient 8	70	M	Asymptomatic	Renal	2	None	Radiation	9
Patient 9	44	F	Asymptomatic	Diffuse Large B Cell Lymphoma	1.5	Lymph nodes, bone marrow	Chemotherapy	Autopsy
Patient 10	74	M	Asymptomatic	Acute Myeloid Leukemia	0.08	Leptomeninges, spinal nerve roots, heart, lung, pancreas, kidneys, GI, liver, spleen, adrenals, skin, soft tissue	None	Autopsy
Patient 11	72	F	Asymptomatic	Renal	0.25	Brain, bilateral kidneys, adrenal, liver, bone	Radiation, immunotherapy, targeted therapy	Autopsy

Figure 1 - 1101

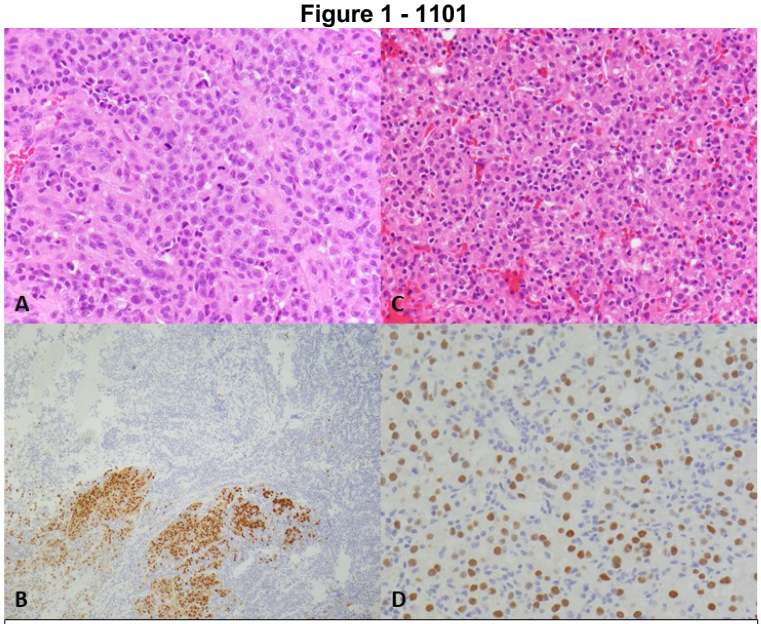

Figure 1: Metastatic pituitary tumors: (A) Metastatic melanoma to pituitary adenoma: Tumor composed of pleomorphic cells with eosinophilic cytoplasm and prominent nucleoli (400x). Numerous mitotic figures are present. These cells show nuclear expression of MITF (B), while the adenoma cells are negative (100x). (C) Metastatic renal cell carcinoma: Tumor composed of sheets of cells with finely vacuolated eosinophilic cytoplasm (400x). (D) The cells demonstrate positive nuclear staining with PAX8 (400x).

Figure 2 - 1101

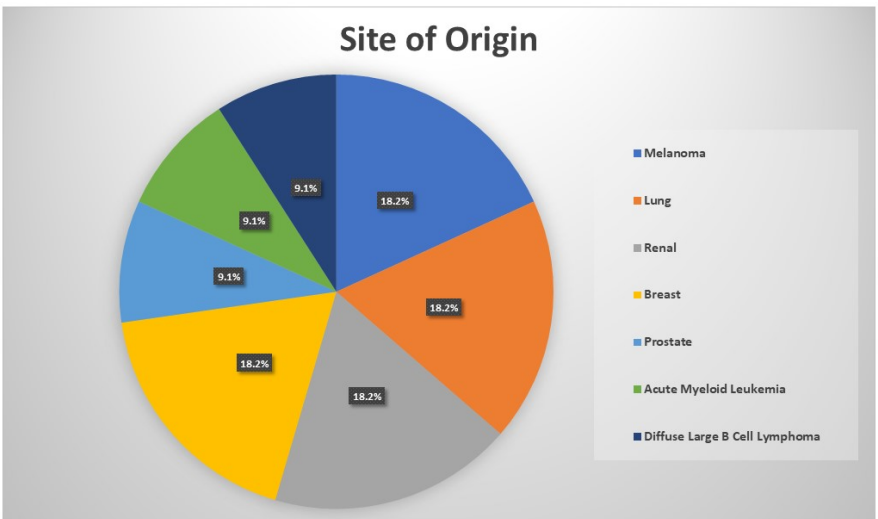

Figure 2: Metastatic Pituitary Lesions by Site of Origin: The most common sites of origin in our series were lung, breast, renal and melanoma, followed by prostate, acute myeloid leukemia and diffuse large B cell lymphoma.

Conclusions: Metastatic lesions of the pituitary are rare and account for only a small fraction of pituitary tumors. In our series, the most common sites of origin were lung, kidney and breast, which is similar to those reported in the literature. As demonstrated by our series, pituitary metastases may be the initial presentation of malignancy and can clinically mimic pituitary adenoma. In some cases, pituitary adenomas and metastases may co-exist, further complicating the histopathological diagnosis. Awareness of this rare event is necessary for pathologists to direct appropriate immunohistochemical work-up in cases with unexpected morphology in pituitary lesions.

1102 Clinical Application of Next Generation Sequencing in Glioblastoma : An Institutional Experience

Xiaomo Li[1], Elias Makhoul[1], Saleh Heneidi[1], Serguei Bannykh[1], Jean Lopategui[2], Eric Vail[1], Xuemo Fan[1]
[1]Cedars-Sinai Medical Center, Los Angeles, CA, [2]Cedars-Sinai Medical Center, West Hollywood, CA

Disclosures: Xiaomo Li: None; Elias Makhoul: None; Saleh Heneidi: None; Serguei Bannykh: None; Jean Lopategui: None; Eric Vail: *Speaker*, Bayer, Eli Lilly, Illumina, Thermo Fisher; *Consultant*, PierianDx; *Employee*, LungLifeAI; Xuemo Fan: None

Background: Glioblastoma is the deadliest type of primary brain tumor characterized by a very poor prognosis, low overall survival rate, and a high recurrence rate. The current treatment, which has remained largely unchanged for the last decade, is surgical resection followed by radiotherapy and temozolomide. Next generation sequencing (NGS) of tumor samples has offered diagnostic, prognostic and therapeutic information to pathologists and oncologists to better categorize and treat patients. Unfortunately, the integration of NGS in glioblastoma treatment algorithms is not yet standard of practice. In our medical center, we routinely perform a 161 gene NGS panel for all glioblastoma cases. Herein, we present our experiences with NGS in this cohort and address its clinical utility in managing oncologic patients.

Design: A total of 205 cases with glioblastoma were selected. A 161 Oncomine Comprehensive Assay V3M, targeting hotspot mutations for SNVs, indels, amplifications, and fusions were performed on tumor specimens. Key parameters included gene alterations, clinical outcomes, and actionability. The genetic alterations were categorized according to eligibility for FDA-approved drugs for patient's tumor type, FDA-approved drugs for other indications (off-label use), or clinical trial eligibility.

Results: Of the 205 cases submitted to our department, all cases were found to have at least one actionable genomic abnormality eligible for the current open phase II clinical trial. GBM associated signal pathways including RTK/RAS/PI3K, P53 and Rb are detected frequently. There are 63 cases with EGFR mutation, 96 cases with TERT mutation, 82 cases with PTEN mutation, 3 cases with KRAS mutation, 6 cases with FGFR3 mutation, 8 cases with FGFR3/TACC3 translocation, 17 cases with IDH1 mutation, 115 cases with TP53 mutation. 25 cases with CDK4 amplification, 27 cases with CCND2, MDM2, MDM4 amplification. These molecular aberrations are frequent drivers in GBM signaling pathways and are all targetable.

Conclusions: In all the cases in our cohort, NGS was able to provide diagnostically, prognostically and therapeutically relevant information. We conclude that NGS can be a useful tool for guiding patient management for the WHO grade IV glioblastoma. Further work is needed to determine whether NGS is changing patient management and improving clinical outcomes.

1103 Prevalence of Limbic Predominant Age-Related TDP-43 Encephalopathy in a Community Based Autopsy Service

M. Beatriz Lopes[1], Tiffany Wang[2]
[1]University of Virginia Health System, Charlottesville, VA, [2]University of Virginia School of Medicine, Charlottesville, VA

Disclosures: M. Beatriz Lopes: None; Tiffany Wang: None

Background: Limbic predominant age-related TDP-43 encephalopathy (LATE) is a newly recognized neurodegenerative disease (NDD) that resembles Alzheimer disease (AD)-type dementia of the oldest-old. The major protein involved in LATE is phosphorylated TDP-43 (pTDP-43). The incidence of LATE neuropathological change (LATE-NC) has been primarily studied in AD research cohorts, where it has been found in 20-50% of individuals on autopsy (1). We sought to determine the burden of LATE-NC in a general community based autopsy service.

Design: 42 autopsy brains from subjects ≥ 75 years between 2014-2020 were selected according to institutional IRB protocol. 19 subjects had clinical history of dementia, with 16 confirmed to have a diagnosis of a NDD by autopsy. 23 subjects had no clinical dementia, with 3/23 having a NDD diagnosed only by autopsy. Sections of the hippocampus and amygdala were stained with an anti-pTDP-43 antibody (Clone 1D3/TDP-43; Covance catalog# SIG-39852). The slides were assessed for pTDP-43 accumulation in neurites, neuronal cytoplasm or nuclei (1) blindly of clinical history and/or autopsy diagnosis.

Results:
12 of the 42 cases (28.57%) were positive for pTDP-43. 9/12 positive cases were from subjects with clinical dementia and diagnosis of a NDD by autopsy (47.37% of the cases with dementia). The remaining 3 positive cases were among 20 subjects without clinical dementia or diagnosis of a NDD by autopsy (13.04% of the subjects without dementia). Of the 9 positive cases with clinical dementia, pTDP-43 staining was present in both hippocampus and amygdala in 6 cases, 2 in the amygdala only, and 1 in

the hippocampus only. In patients without clinical dementia, 2 showed pTDP-43 positivity in the hippocampus alone, and one in the amygdala only.

Conclusions: While LATE-NC is found at higher rates among subjects with clinical dementia, the incidence among the general population is not insignificant, with 13.04% having LATE pathology despite lack of dementia or diagnosis of a NDD. Our findings also demonstrate that in the general community, the incidence of LATE-NC is relatively high at 28.57%. Further studies on a larger group of subjects will determine the burden that LATE may have on public health as the population ages.

(1) PMID: 31039256

1104 Next-Generation Sequencing Findings Support a Divergent Clonal Evolution in Composite Pleomorphic Xanthoastrocytoma-Ganglioglioma

Calixto-Hope Lucas[1], Christian Davidson[2], Angelica Putnam[3], Joe Mendez[2], Carol Bruggers[2], Nicholas Whipple[2], Daniel Sullivan[1], Biswarathan Ramani[1], Cathryn Cadwell[1], Joanna Phillips[1], Jessica Van Ziffle[1], Walter Devine[1], David Solomon[1], Arie Perry[1]

[1]University of California, San Francisco, San Francisco, CA, [2]University of Utah Health, Salt Lake City, UT, [3]The University of Utah, Salt Lake City, UT

Disclosures: Calixto-Hope Lucas: None; Christian Davidson: None; Angelica Putnam: None; Joe Mendez: None; Carol Bruggers: None; Nicholas Whipple: None; Daniel Sullivan: None; Biswarathan Ramani: None; Cathryn Cadwell: None; Joanna Phillips: None; Jessica Van Ziffle: *Stock Ownership*, Adaptive Biotechnologies; Walter Devine: None; David Solomon: None; Arie Perry: None

Background: Composite pleomorphic xanthoastrocytoma-ganglioglioma (PXA-GG) is an extremely rare CNS neoplasm that exhibits two distinct but intermingled components. It is unknown whether this tumor represents a “collision tumor” of separate neoplasms or divergent evolution from a single common precursor.

Design: Capture-based next-generation sequencing targeting the coding regions of 479 cancers genes, select introns, and the TERT promotor was performed on extracted DNA from three PXA-GG. Single nucleotide variants, insertions/deletions, copy number alterations, and selected rearrangements were evaluated. Analysis of a fourth PXA-GG is in progress.

Results: Three PXA-GG were diagnosed in 1 male and 2 female patients ranging from 15.4 to 18.9 years in age. Locations included the temporal lobe, parietal lobe, and cerebellum. DNA was sufficient for analysis in three PXA components and two GG components. All PXA and GG components analyzed harbored BRAF p.V600E hotspot mutations. The GG component with insufficient material for sequencing was BRAF V600E mutant protein positive by immunohistochemistry. All PXA components demonstrated CDKN2A homozygous deletion by sequencing with loss of p16 expression by immunohistochemistry, which was intact in all GG components. One PXA component additionally harbored a TERT c.-124C>T promotor hotspot mutation. The PXA components also demonstrated increased copy number changes relative to their paired GG components. In one PXA-GG, common chromosomal copy number alterations were identified in both components.

Conclusions: We identify common BRAF hotspot mutations in both components of PXA-GG, and CDKN2A homozygous deletion exclusive to the PXA component. Additionally, one case demonstrated similar chromosomal copy number alterations across both PXA and GG components. These findings support divergent evolution of the PXA component from a precursor BRAF p.V600E-mutant GG, with additional acquisition of CDKN2A homozygous deletion as is typically seen in conventional PXA.

1105 Orbital and Periorbital Metastases of Breast Cancer: An Academic Institutional Experience

Emily Mejia[1], Vincent Tang[2], Sander Dubovy[2], Carmen Gomez-Fernandez[1]

[1]University of Miami Miller School of Medicine, Miami, FL, [2]Bascom Palmer Eye Institute, Miami, FL

Disclosures: Emily Mejia: None; Vincent Tang: None; Sander Dubovy: None; Carmen Gomez-Fernandez: None

Background: Breast cancer is the most common cancer in women and the most common metastatic sites include bone, lung, brain, and liver. Breast cancer rarely metastasizes to the orbit and periorbit, with an estimated incidence of 1-13%. However, the most common primary site for metastases to the orbit is breast, accounting for approximately 28.5 -58.8% of all orbital metastases.

Herein, we report the largest case series of 34 patients with breast cancer metastases to the orbit and periorbit based on a single academic institution review.

Design: Our pathology database was queried for orbital and periorbital breast cancer metastases from 1999 to the present and 34 cases were retrieved. Cases were reviewed for clinical history and characterized with immunohistochemistry (IHC) for GATA-3, E-cadherin, ER, PR, and HER-2. Slides were reviewed by two board certified anatomic pathologists, one with a subspecialty in breast and one in ophthalmic pathology.

Results: Our cohort included 34 patients with breast cancer metastases to the orbit and periorbital area. The ages ranged from 26-85 (median=66) and all the patients were female. There were 15 (44%) cases occurring in the right orbit, 18 (56%) in the left orbit, and 1 (3%) in an unspecified location (Table). Invasive lobular carcinoma (negative for e-cadherin) represented the majority of the cases (82%) with 8 cases of invasive ductal carcinoma (positive for E-cadherin). Of the total cases, 19(56%) were positive for both ER and PR, 11(32%) were positive for ER and negative for PR, and all cases were negative for HER2. Four cases (12%) were characterized as triple negative breast cancers, including three invasive lobular carcinomas.

Table 1	N (%)
Laterality	
Right	15 (44%)
Left	18 (53%)
Unspecified	1 (3%)
Anatomical Location	
Orbit (total)	28 (82%)
Unspecified	22 (65%)
Lacrimal Gland	3 (9%)
Lateral Rectus	1 (3%)
Medial Rectus	1 (3%)
Optic nerve sheath	1 (3%)
Eyelid	4 (12%)
Conjunctiva (unspecified)	1 (3%)
Unspecified location	1 (3%)

Conclusions: Breast cancer metastasis to the orbit and periorbit is a rare but important differential in the evaluation of orbital masses. Our study represents the largest intuitional case series of metastatic breast carcinoma to the orbit and periorbit. IHC staining patterns suggest the majority of our cases were invasive lobular carcinoma with a small subset being invasive ductal carcinoma. Characterization of these tumors have significant implications for patient diagnosis and treatment.

1106 Diverse Histopathologic Patterns of Intracranial Mesenchymal Tumor with FET-CREB Fusion

Bryan Morales-Vargas[1], Jose Velazquez Vega[2], Matthew Schniederjan[3], Stewart Neill[4]
[1]Emory University School of Medicine, Atlanta, GA, [2]Children's Healthcare of Atlanta, Atlanta, GA, [3]Emory University, Children's Healthcare of Atlanta, Atlanta, GA, [4]Emory University School of Medicine, Decatur, GA

Disclosures: Bryan Morales-Vargas: None; Jose Velazquez Vega: None; Matthew Schniederjan: None; Stewart Neill: None

Background: Intracranial mesenchymal tumors with FET-CREB fusions comprise a recently designated group of neoplasms of the central nervous system; previously, case reports of these tumors described them using variable terminology such as intracranial angiomatoid fibrous histiocytoma. Recently, these have been molecularly defined by in-frame gene fusions of the FET family of RNA-binding proteins (EWSR1 or FUS) to the CREB (cyclic AMP response binding element protein) family of transcription factors (ATF1, CREB1, and CREM). Cases reported were uniformly intraventricular or extra-axial, along the cerebral convexities, falx, lateral ventricles, tentorium, cerebellopontine angle and spinal cord. The histologic features encompass a wide morphologic spectrum with unifying features including a collagenous stroma and dense intercellular matrix.

Design: Immunohistochemistry was performed on whole formalin-fixed, paraffin-embedded tissue sections for GFAP, synaptophysin, EMA, CD99, desmin, S100, MUC4, SSTR2a and HMB45. Next-generation sequencing was performed using an Archer FusionPlex Sarcoma Kit.

Results: Two of our cases displayed unusual morphology and/or immunohistochemical staining. One, in a 33-year-old female with an intraparenchymal left occipital mass resembling a glioma, exhibited tumor cells with glia-like cytoplasmic projections in a myxoid and necrotic background; these tumor cells were strongly positive for GFAP, a unique finding in this entity. An EWSR1-CREM fusion was found in this case. The second, in a 56-year-old female with a left frontal lobe mass, showed scarce epithelioid tumor cells in a perivascular distribution; the lesion was dominated by numerous non-necrotizing granulomata reminiscent of sarcoidosis. An EWSR1-ATF1 fusion was revealed in this case. Other cases in our series, both dural-based, displayed more typical features, with mildly atypical epithelioid and spindled cells set within a collagenous to myxoid stroma. These two cases held EWSR1-CREM fusions. All four cases were positive for desmin and EMA expression.

Conclusions: Intracranial mesenchymal tumors which harbor a FET-CREB fusion have shown a wide range of morphologic features. Here, we present four cases with variable appearances and morphologic findings mimicking other neoplastic and non-neoplastic processes.

1107 Ophthalmic Metastatic Disease: A Retrospective Study of 638 Autopsies

Sepideh Siadati[1], Charles Eberhart[1]
[1]Johns Hopkins University School of Medicine, Baltimore, MD

Disclosures: Sepideh Siadati: None; Charles Eberhart: None

Background: Ocular metastases are more common than primary eye malignancies, and often arise from breast, lung, gastrointestinal tract, and prostate. However, earlier studies were largely based on clinical diagnosis. In this retrospective study, we examine a large series of autopsies in which eyes were examined postmortem in order to compare ocular involvement by malignancy with overall tumor dissemination.

Design: Autopsy records between January 1, 2015 and September 14, 2021 were reviewed in order to identify patients who had died from cancer. At least 4 sections from a pupil-optic nerve block, which included limited optic nerve and soft tissues, were examined for each eye; in most cases both globes were examined.

Results: There were 638 autopsies in which eyes were examined, including 229 with a diagnosis of malignancy. Of the 229 patients who died with malignancy, 141 (62%) had either an antemortem or autopsy diagnosis of metastatic disease at some body site. Among these, we found 17 patients whose globes or adherent tissues were involved, including 5 with leukemia/lymphoma diagnosed outside the eye. These represented 9 females (32 to 76 years old, mean 54) and 8 males (17 to 79 years old, mean 56). The most common location for metastasis was choroid (10 cases, 59%) followed by optic nerve/leptomeninges (4 cases, 23%), extraocular muscles (1 case, 6%), sclera (1 case, 6%), and orbital fat (1 case, 6%). Seven out of 10 choroidal metastases involve both eyes, while all 4 cases with involvement of optic nerve/leptomeninges were bilateral. The most common non-primary malignancy identified in the globe or adjacent optic nerve was breast carcinoma in females (5 cases) and leukemia/lymphoma in males (4 cases). Other tumor types were lung adenocarcinoma (2 cases, and one case each of colon adenocarcinoma, prostatic adenocarcinoma, squamous cell carcinoma of bladder, endometrioid carcinoma, osteosarcoma, and neuroendocrine carcinoma. Of the non-hematological malignancies, 11 out of 12 (92%) had been diagnosed antemortem with metastases. However, in only one of these 11 cases had spread to the eye been identified clinically before death.

Conclusions: In 229 autopsied patients with malignancies arising outside the eye, 17 (7%) had spread to the globe or adjacent tissues at the time of death. In all but one case, this had not been identified clinically before death, suggesting the eye may be an underappreciated metastatic site in advanced cancer patients.

1108 NTRK Fusion in Japanese Central Nervous System Tumors

Ayako Ura[1], Keita Sasa[1], Takuo Hayashi[2], Takashi Yao[3], Tsuyoshi Saito[4]
[1]Juntendo University, Bunkyo-ku, Japan, [2]Juntendo University Graduate School of Medicine, Tokyo, Japan, [3]Juntendo University, Tokyo, Japan, [4]Juntendo University, School of Medicine, Tokyo, Japan

Disclosures: Ayako Ura: None; Keita Sasa: None; Takuo Hayashi: None; Takashi Yao: None; Tsuyoshi Saito: None

Background: *NTRK* fusions have been reported to be rare in cancers across various organs, except for certain types of tumors such as infantile fibrosarcoma and secretory adenocarcinoma of breast and salivary gland. *NTRK* fusion positive tumors are reported to be highly sensitive to TRK inhibitors such as Larotrectinib and Entrectinib. It is very important to identify patients who may benefit from these inhibitors. In central nervous system (CNS) tumors, especially gliomas, the frequency of *NTRK* fusions has been reported to be approximately 2%, however, the frequency of *NTRK* fusions in CNS tumors of Japanese patients is unknown. Pan-trk antibody is shown to be useful to identify *NTRK* fusion tumors, however, the physiological expression of NTRKs in neural tissues hamper the identification of CNS tumors with *NTRK* fusion. In this study, we employed quantitative PCR (qPCR)-based screening system of *NTRK* fusions in CNS tumors by evaluating the imbalanced expression of *NTRK1-3*.

Design: We performed Real-time qPCR for *NTRK1*, *NTRK2* and *NTRK3* in 390 Japanese cases with CNS tumors. Primers and probes were designed to recognize each 5'-side and 3'-side of *NTRK1-3*. Cases with imbalanced expression for either *NTRK1-3* were further analyzed using Nanostring gene expression assay containing probes for each 5'-side and 3'-side of *NTRK1-3.* Cases showing imbalanced expression by both analysis were sent for target RNA sequences.

Results: Totally, 35 CNS tumors showed imbalanced expression by real-time qPCR for either NTRK1-3 (24 *NTRK1*, 7 *NTRK2*, 8 *NTRK3*). *NTRK* fusion were confirmed by RNA sequencing in only one cases [*CKD5RAP2-NTRK2*, i.e., 1/390 (0.3%)]. Clinicopathologically, histological type of this case was glioblastoma, and this patient died from aspiration pneumonia 10 months after surgery.

Conclusions: This is the first report regarding the frequency of *NTRK* fusion in Japanese CNS tumors. Given the high mortality rate of patients with unresectable glioblastomas, TRK inhibitors could be an efficient molecular target therapy. Real-time qPCR testing for imbalanced expression of either *NTRK1-3* could contribute to find patients with CNS tumors who can benefit from TRK inhibitors. It is necessary to await the accumulation of positive cases to clarify the frequency and the biological behavior of CNS tumors with *NTRK* fusion.

1109 Higher Frequency of Acute and Subacute Postmortem Neuropathologic Findings in Patients with COVID-19 Infection

Michael Williams[1], Rati Chkheidze[2], Richard Powers[1]
[1]UAB Hospital, Birmingham, AL, [2]The University of Alabama at Birmingham, Birmingham, AL

Disclosures: Michael Williams: None; Rati Chkheidze: None; Richard Powers: None

Background: Increasing numbers of COVID-19 patients experience acute and chronic neurologic symptoms and complications. Despite ample clinical evidence of CNS involvement by COVID-19, reported neuropathological findings in the postmortem brain tissues of COVID19 patents include variety of hypoxic/ischemic changes, thrombosis, intracerebral and subarachnoid hemorrhage, nonspecific microglial activation and/or lymphocytic infiltration. But, there is no clear evidence whether these findings are specific to COVID19 infection or not.

Design: Autopsy brains specimens from 94 COVID19 patients and 61 controls (COVID 19 negative PCR test at time of autopsy) were examined. Clinical data on the presence of comorbid conditions, such as hypertension, diabetes, hyperlipidemia, chronic cardiac, and renal disorders were collected for both groups. Using routine neuropathology approaches, the extents of vascular pathology; acute, subacute, and remote ischemic hemorrhagic lesions; microvascular thrombosis, cerebral edema, and intraparenchymal and subarachnoid hemorrhage were examined. For histopathologic examination hippocampus, frontal and parietal neocortices and white matter, basal ganglia, midbrain, pons, medulla, and cerebellum were selected.

Results: Mean age in the COVID19 group was 63 years and 60 years in the control group. There were more males in both group than females (COVID19 – 2.8:1, Control – 1.5:1). There was no statistically significant difference between groups in the frequencies of systemic comorbid conditions. 93% of COVID19 cases and 87% of control cases had at least one gross and/or microscopic neuropathologic finding. COVID19 cases showed higher rate of combined acute findings, including brain edema, acute and

subacute hypoxic/ischemic lesions, thrombosis, and hemorrhage (61% vs 39%, P value – 0.002). When compared these features separately, none of them reached statistical significance. Arteriolosclerosis (66% vs 66%), atherosclerosis (17% vs 26%), and remote infarcts (19% vs 18%) where quite common findings with similar frequencies in both groups.

Conclusions: Our data shows higher tendency of acute and subacute events in the patients with COVID19 infection. These finding do not quite explain the clinical symptoms seen in patients with neurologic complications, and likely represent the sequela of COVID19 systemic complications. More comprehensive neuropathologic and molecular approaches are necessary to better understand the mechanisms of neurologic complications of COVID19 infection.

1110 Marked Up-Regulation of the Transcription Co-Factor SAP30 mRNA in Ischemic Stroke

Yue Yang[1], Xian-Long Wen[1], Ming-Jie Li[1], Hong-Bo Pan[1], Zhi-Guang Huang[1], Ying-Dan Zhang[1], Tao Wei[2], Gui-Miao Jiang[1], Hui Cai[1], Kun-Feng Chen[1], Hai-Cheng Li[1], Jia-Feng Chen[1], Li Chen[1]
[1]The First Affiliated Hospital of Guangxi Medical University, Nanning, China, [2]Liuzhou, China

Disclosures: Yue Yang: None; Xian-Long Wen: None; Ming-Jie Li: None; Hong-Bo Pan: None; Zhi-Guang Huang: None; Ying-Dan Zhang: None; Tao Wei: None; Gui-Miao Jiang: None; Hui Cai: None; Kun-Feng Chen: None; Hai-Cheng Li: None; Jia-Feng Chen: None; Li Chen: None

Background: Ischemic stroke (IS) is the major type of stroke where hypoxia inflicts. Previous observation in genome-wide binding profiles has shed light on the transcriptional repression activity of SAP30 in response to hypoxia. However, expression level of the transcription co-factor SAP30 in IS settings remains to be elucidated. We aimed to investigate the mRNA level of SAP30 and its possible transcription repression mechanisms in IS.

Design: First, standardized mean differentiation (SMD) was used to comprehensively evaluate the mRNA level of SAP30 in IS from datasets published on public genomics repositories. Next, the area under the curve (AUC) of summary receiver operating characteristic (SROC) curve was evaluated. We then looked into the pathways in which the negatively-coexpressed differentially expressed target genes (DETGs) of SAP30 were involved. Last, prominent negatively-coexpressed DETGs that showed the highest tendency to be bound by SAP30 during transcription activity were discussed in detail to probe the potential transcriptional repression mechanisms SAP30 was endowed with in neuropathology.

Results: A total of 10 datasets (251 IS cases and 100 controls) were included in our study. SAP30 mRNA level was markedly up-regulated in IS (SMD = 1.00, 95% CI: 0.75~1.25, $P < 0.01$). AUC of SROC for SAP30 was 0.86, showing considerable ability to distinguish IS from non-IS. Negatively co-expressed DETGs of SAP30 were significantly enriched in transcriptional activities. After detailed discussion of 3 prominent negatively-coexpressed DETGs - ABLIM1, ZNF589 and PIK3C2B, and one neurotrophic factor - NOG, SAP30 was assumed an adverse factor through transcription repression of neuroprotectors.

Comprehensive analysis of SAP30 mRNA expression in ischemic stroke (IS) from all datasets.

Study ID	IS			Normal			SMD	95% CI
	n	Mean	SD	n	Mean	SD		
GSE109233	7	9.22	0.630	7	8.83	0.287	0.75	-0.35; 1.84
GSE122709	10	6.47	0.415	5	5.65	0.196	2.12	0.73; 3.51
GSE140275	3	5.76	0.216	3	6.04	0.200	-1.10	-3.02; 0.82
GSE158312	20	7.94	0.381	4	7.81	0.376	0.34	-0.74; 1.42
GPL6883	107	9.98	0.660	24	9.28	0.371	1.12	0.66; 1.58
GPL570	97	5.86	0.343	51	5.50	0.287	1.12	0.75; 1.48
GSE56267	7	7.29	0.181	6	7.24	0.210	0.22	-0.88; 1.31
Overall	251			100			1.00	0.75; 1.25

($I^2 = 0.47$,

$P = 0.08$)

ISIS: ischemic stroke; n: number; SD: standard deviation; SMD: standardized mean difference; CI: confidence interval.

Figure 1 - 1110

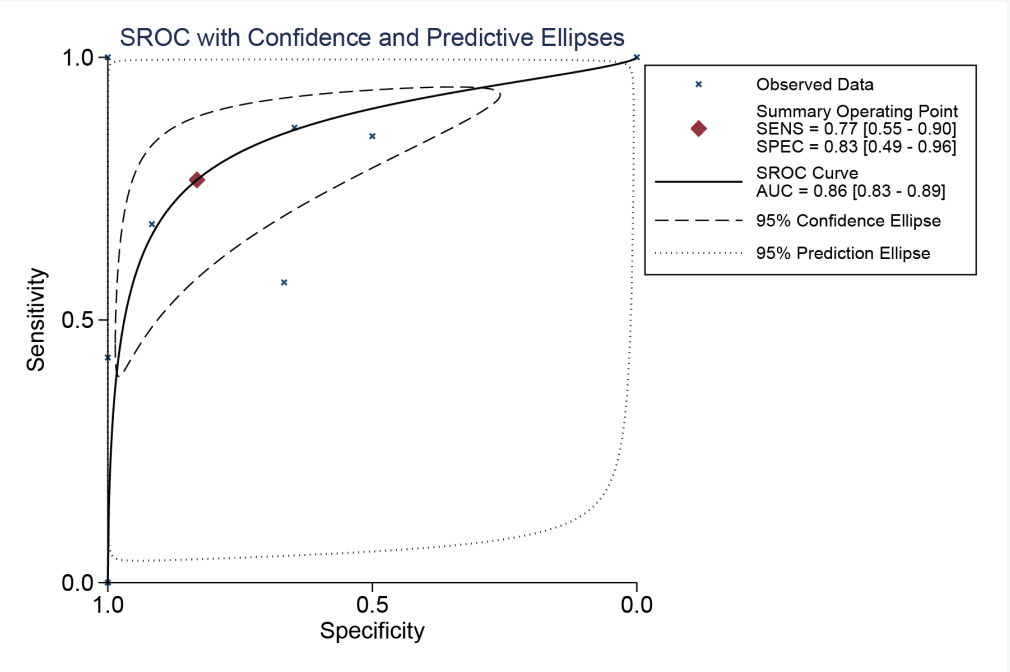

Figure 2 - 1110

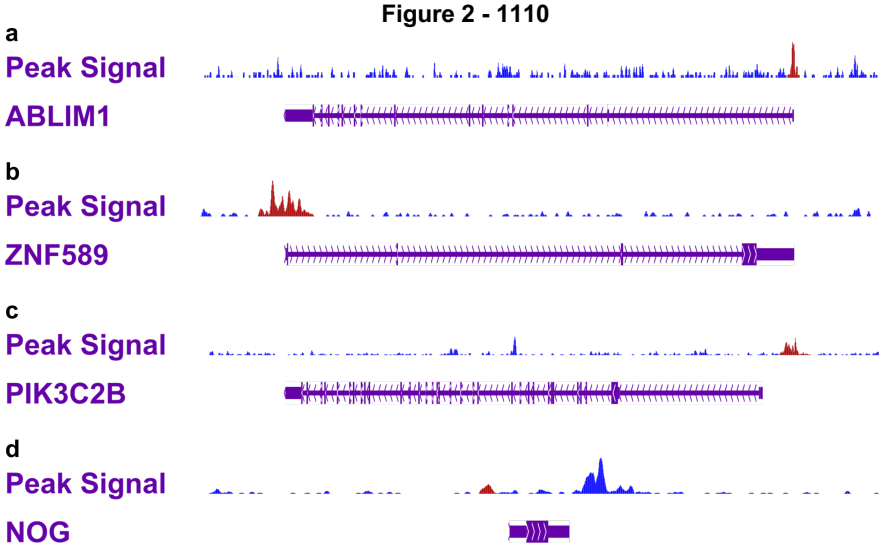

Conclusions: This study utilized 10 datasets of IS of human species available across GEO and ArrayExpress, encompassing 251 IS cases and 100 controls, to pilot a comprehensive demonstration that SAP30 mRNA was significantly up-regulated under IS conditions, and to propose SAP30 to be a prospective IS biomarker. SAP30 may suppress ABLIM1, ZNF589, PIK3C2B and NOG to exert a neuropathological role.